

# An Experimental Investigation of the Steady-State Response of a Noncontacting Flexibly Mounted Rotor Mechanical Face Seal

**An Sung Lee**

Korea Institute of Machinery and Metals,  
Daejeon 305-600, Korea

**Itzhak Green<sup>1</sup>**

George W. Woodruff School  
of Mechanical Engineering,  
Georgia Institute of Technology,  
Atlanta, GA 30332-0405

*Recent theoretical work on the dynamics of the noncontacting flexibly mounted rotor (FMR) seal has shown that it is superior in every aspect of dynamic behavior compared to the flexibly mounted stator (FMS) seal. The FMR seal is inherently stable regardless of the operating speed, the maximum relative misalignment response is smaller, and the critical stator misalignment is larger. All these are measures of superior performance. This work undertakes the experimental investigation of the dynamic behavior of a noncontacting FMR seal. The steady-state response of the FMR seal was measured at various operating conditions. The results are given in terms of dynamic and static transmissibilities, i.e., amplitude ratio of responses to two forcing inputs: the initial rotor and fixed stator misalignments. These are then compared to the analytical predictions. Further, operation maps are drawn for each set of operation conditions. The maps indicate how safely (away from contact) the seal operates. It is shown that the combination of the seal parameters that maximize the fluid film stiffness is optimal for safe noncontacting operation.*

## Introduction

Mechanical face seals are commonly used in sealing rotating shafts in turbomachinery where tightly controlled leakage rates are frequently imposed. They have experienced a rapid growth especially in applications such as primary coolant pumps (PCP) of nuclear power plants, jet engine compressors, and pumps handling liquefied petroleum gases. Extreme operating conditions in modern high performance turbomachinery of high speeds, pressures, and temperatures require the utilization of noncontacting mechanical face seals, even in cases of hazardous fluids. Recent work by Salant and Blasbalg (1991) and Yasuna and Hughes (1992) investigated the dynamics of two-phase seals where the lubricating film may flash because of pressure drop in a high temperature environment. These, however, were theoretical studies limited to a single axial degree of freedom. To ensure long life and reliable operation the seal must also be inherently stable, particularly in the angular mode, and its angular steady-state response should be such that wear and leakage are minimum.

Knowledge progressed from observation of various phenomena (Denny, 1961) to theoretical investigations (Etsion, 1991). Currently, theoretical predictions have progressed to the point where they have to be evaluated experimentally. Particularly, Green (1989, and 1990) completed the theoretical

analysis of a noncontacting FMR mechanical face seal (Fig. 1) from a rotordynamics point of view. The FMR seal was found to be free of instabilities, if the rotor is a "short disk," and the steady-state solution was given in terms of transmissibilities, i.e., amplitude ratio of responses to forcing inputs. As suggested by Metcalfe (1981), and theoretically proven by Green (1989), the FMR seal is a better design than the flexibly mounted stator (FMS) seal (Green and Etsion, 1985) for high performance applications. While it is worth noting that FMS and FMR seals are about equally used in various industries, no experimental investigation of the dynamic response of the FMR seal has been reported.

To simulate physically the steady-state response of an FMR seal and to assess the theoretical results an experimental program was carried out, where features of the test rig (Fig. 2) and methods of data analysis were discussed in detail in Lee and Green (1994a), and in whole in Lee (1992). Obstacles in the rig performance have been identified and eliminated (Lee and Green, 1994b). Since in the test rig the FMR seal was mounted on a shaft, its dynamic behavior was expected to be somewhat influenced by the shaft dynamics. The analytical results (Green, 1989), however, were obtained assuming that the shaft is perfectly rigid. Therefore, before comparisons between the experimental and theoretical results can be made, the effect of the shaft dynamics on the seal response had to be known. Using the complex extended transfer matrix method (Lee and Green, 1994c) the dynamics of the shaft and seal were coupled. The method was applied to the rig of interest where results showed that the effects of the shaft flexibility was practically negligible. Hence, the dynamic responses of

<sup>1</sup>On leave until July 31, 1994, at: Technion-Israel Institute of Technology, Faculty of Mechanical Engineering, Haifa 32000, Israel.

Contributed by the Tribology Division of THE AMERICAN SOCIETY OF MECHANICAL ENGINEERS and presented at the ASME/STLE Tribology Conference, Maui, Hawaii, October 16-19, 1994. Manuscript received by the Tribology Division March 1, 1994; revised manuscript received June 14, 1994. Paper No. 94-Trib-25. Associate Technical Editor: R. F. Salant.

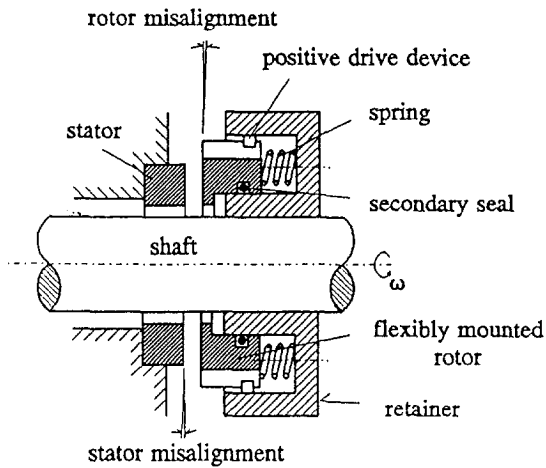


Fig. 1 Schematic of a noncontacting flexibly mounted rotor (FMR) mechanical face seal

the FMR seal as measured from the test rig can be compared directly to the analytical predictions by Green (1989). Also, since the ratio  $I_r/I_p = 0.674$  (rotor transverse moment of inertia over polar moment of inertia) is less than one, stability was guaranteed.

In this work the experimental results of the noncontacting FMR seal will be given at each set of operating conditions in the following three categories: (1) dynamic transmissibility, (2) static transmissibility, and (3) operation map.

**Transmissibilities.** Stator and rotor misalignments are defined in Fig. 1. The dynamic transmissibility,  $\gamma_{rl}/\gamma_{ri}$ , is the amplitude ratio of the rotor angular response to its own initial misalignment. The static transmissibility,  $\gamma_{rs}/\gamma_s$ , is the amplitude ratio of the rotor angular response to the fixed stator misalignment. The transmissibilities obtained analytically by Green (1989) are:

$$\gamma_{rs} = \frac{\sqrt{K_f^2 + \frac{1}{4} D_f^2 \omega^2}}{\sqrt{(K_s + K_f)^2 + \left(D_s \omega + \frac{1}{2} D_f \omega\right)^2}}$$

$$\gamma_{rl} = \frac{K_s}{\sqrt{[(I_p - I_r) \omega^2 + (K_s + K_f)]^2 + \left(\frac{1}{2} D_f \omega\right)^2}}$$

(1)

The experimentally obtained transmissibilities will be compared to the analytical ones (see Nomenclature for definitions). The details of calculating various parameters and numerical data are given in the Appendix.

## Nomenclature

$C$  = seal clearance  
 $D_f$  = fluid film damping  
 $D_s$  = support damping  
 $I_p$  = polar moment of inertia  
 $I_r$  = transverse moment of inertia  
 $K_f$  = fluid film stiffness  
 $K_s$  = support stiffness  
 $p$  = water pressure  
 $Q$  = leakage  
 $r_i$  = seal inner radius

$r_o$  = seal outer radius  
 $R_i$  = dimensionless inner radius,  $r_i/r_o$   
 $R_m$  = dimensionless mean radius,  $(1 + R_i)/2$   
 $\beta$  = coning angle  
 $\beta$  = dimensionless coning,  $\beta r_o/C$   
 $\bar{\gamma}$  = relative misalignment between rotor and stator

$\bar{\gamma}$  = dimensionless relative misalignment,  $\gamma r_o/C$   
 $\gamma_{ri}$  = initial rotor misalignment  
 $\gamma_{rl}$  = rotor angular response to  $\gamma_{ri}$   
 $\gamma_s$  = fixed stator misalignment  
 $\gamma_{rs}$  = rotor angular response to  $\gamma_s$   
 $\mu$  = viscosity  
 $\omega$  = shaft speed

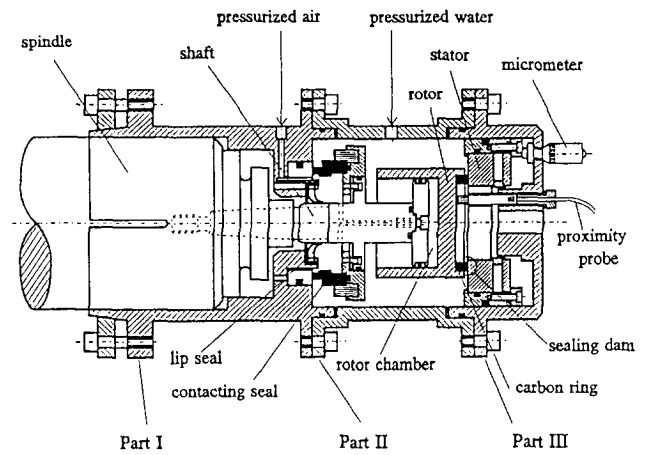


Fig. 2 Schematic of an FMR seal test rig

**Operation Map.** The methods of data analysis and analytical results of the FMR seal assume noncontacting operation. Therefore, it is important to ensure that experimental data was obtained under noncontacting conditions, and to estimate how safely away from contact the seal operated. Contact criteria were thoroughly discussed by Green (1987). For a dimensionless coning,  $\beta$ , that is greater than the critical coning,  $1/R_i$ , face contact occurs at the inner radius, for which the contact criterion is

$$1 - (\bar{\gamma})_{\max} R_i = 0 \quad (2)$$

where  $\bar{\gamma}$  is the dimensionless relative misalignment between the rotor and the stator. Since the dimensionless conings testing here were greater than the critical value ( $1/R_i = 1.25$ ) the above criterion applies.  $(\bar{\gamma})_{\max}$  can be obtained from Green (1989)

$$(\bar{\gamma})_{\max} = |\gamma_{rl}| + \gamma_{rs} - \gamma_s \quad (3)$$

The operation map is drawn giving the value of  $1 - (\bar{\gamma})_{\max} R_i$  as a function of various operating conditions. In this map,  $1 - (\bar{\gamma})_{\max} R_i \leq 0$  indicates contacting operation, whereas  $0 < 1 - (\bar{\gamma})_{\max} R_i \leq 1$  indicates noncontacting operation. The closer the value of  $1 - (\bar{\gamma})_{\max} R_i$  is to 1, the safer the seal operation.

## Operating Conditions and Test Procedures

Each operating condition of the FMR seal was a combination of the following parameters:  $\beta$  (coning angle),  $\gamma_s$  (fixed stator misalignment),  $\gamma_{ri}$  (initial rotor misalignment),  $\omega$  (shaft speed),  $C$  (seal clearance),  $p$  (water pressure), and  $Q$  (leakage rate at the sealing dam). Two values of  $\beta$ , large and small, were tested along with large and small values of  $\gamma_s$ . For a given set of  $\beta$  and  $\gamma_s$ , there were four operating conditions:

- (1) varying  $\omega$ , keeping  $C$  and  $p$  constant
- (2) varying  $C$ , keeping  $\omega$  and  $p$  constant
- (3) varying  $p$ , keeping  $\omega$  and  $C$  constant
- (4) varying  $p$ , keeping  $\omega$  and  $Q$  constant

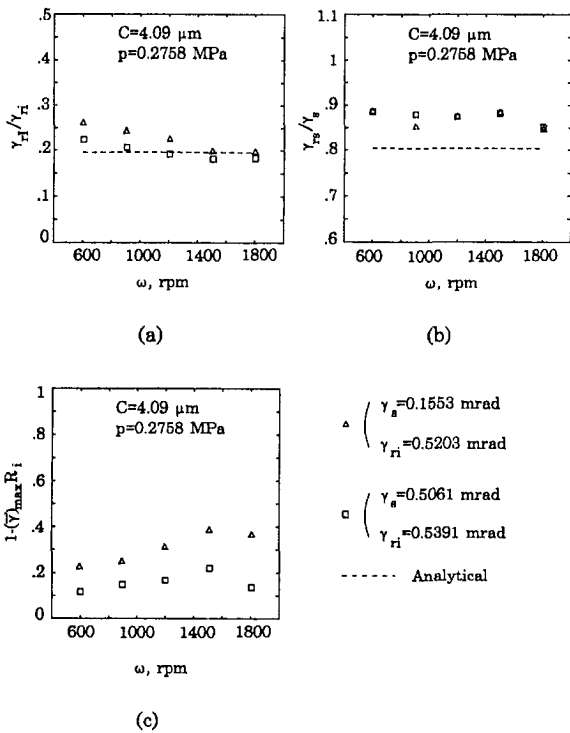


Fig. 3 (a) Dynamic transmissibility, (b) static transmissibility, and (c) operation map for  $\beta = 11.209$  mrad when  $\omega$  varies, keeping  $C = 4.09 \mu\text{m}$  and  $p = 0.2758$  MPa constant

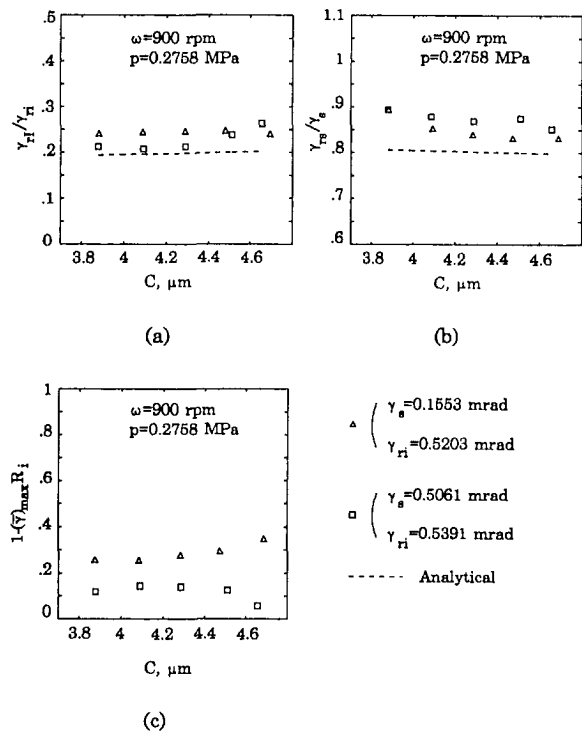


Fig. 4 (a) Dynamic transmissibility, (b) static transmissibility, and (c) operation map for  $\beta = 11.209$  mrad when  $C$  varies, keeping  $\omega = 900$  rpm and  $p = 0.2758$  MPa constant

Condition (4) is equivalent to a case where  $p$  increases and  $C$  decreases to maintain a constant leakage,  $Q$ , at a given speed,  $\omega$ . The conditions described above generate a total of 16 test cases.

All the features of the test rig and data analysis have been described thoroughly in Lee and Green (1994a). For each of the operating conditions described above, the coning,  $\beta$ , could be varied through mechanical deformation, and it was measured by a dial indicator. The forcing inputs,  $\gamma_{ri}$  and  $\gamma_s$ , were measured in static tests. The speed,  $\omega$ , was checked by a digital feedback controller. The water pressure,  $p$ , was measured by a pressure gauge. The leakage,  $Q$ , at a given  $p$  was measured by a flow meter. Fine tuning of  $Q$  accomplished a resolution of  $\pm 0.0278$  cc/s (by controlling the air pressure in the rotor chamber). Then,  $C$  was calculated from the measured  $Q$ . The rotor response was measured by three proximity probes. The measured responses were sampled and stored by the data acquisition system, and analyzed by the methods described in the aforementioned reference. The support and fluid film rotor-dynamic coefficient, which are required for calculating the analytical transmissibilities in Eq. (1), are summarized in the Appendix.

## Results and Discussions

Every result point that follows represents an average taken from five measurements. Results are given for two values of  $\beta$ , large and small. The trends between the experimental and theoretical results are expressed by the correlation coefficient,  $r$ .  $r_1$  represents the correlation coefficient for a small value of  $\gamma_s$ , and  $r_2$  represents the correlation coefficient for a large value of  $\gamma_s$ . The differences between the experimental and theoretical results are expressed by  $e_1$  for a small value of  $\gamma_s$ , and  $e_2$  for a large value of  $\gamma_s$ .

**Large Coning.** The coning,  $\beta$ , was set to 11.209 mrad ( $\beta = 69.44$  for  $C = 4.1 \mu\text{m}$ ). A small value,  $\gamma_s = 0.1553$  mrad,

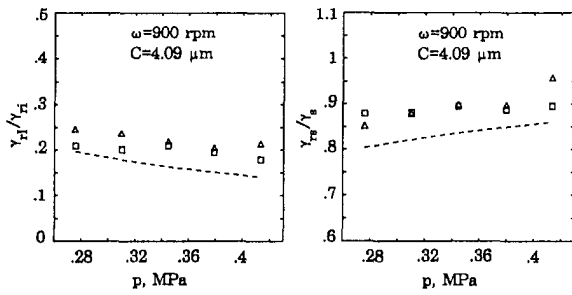
was tested with  $\gamma_{ri} = 0.5203$  mrad, and a large value,  $\gamma_s = 0.5061$  mrad, was tested with  $\gamma_{ri} = 0.5391$  mrad.

Results for  $\omega = 600$  to 1800 rpm in increments of 300 rpm, keeping  $C = 4.09 \mu\text{m}$  and  $p = 0.2758$  MPa constant, are shown in Figs. 3(a), 3(b), and 3(c) for  $\gamma_{ri}/\gamma_{ri}$ ,  $\gamma_{rs}/\gamma_{rs}$ , and the operation map, respectively. The experimental ratio  $\gamma_{ri}/\gamma_{ri}$  (shown by the triangle symbol  $\Delta$  for the small  $\gamma_s$ , and the square symbol  $\square$  for the large  $\gamma_s$ ) decreases as  $\omega$  increases. This is due to the gyroscopic effect (Green, 1989). The analytical  $\gamma_{ri}/\gamma_{ri}$  (shown by the dashed line), however, is slightly increasing. It is presumed that stiffness hardening of the O-rings is causing this effect by acting against the gyroscopic couple. The correlation coefficients are  $r_1 = -0.056$  and  $r_2 = -0.264$ .

The faulty correlation may be explained as follows. In the test rig, the temperature increased due to friction-induced heat at the contacting seal, especially at the higher speeds. The increasing temperature has an inverse effect on the elastomer stiffness, i.e., causes softening of the O-rings. The stiffness calculated by Eq. (A1) in the Appendix originated from a relaxation test performed at a constant room temperature. Since the temperature was not controlled during testing of the FMR seal, Eq. (A1) overestimates the actual O-rings stiffness, and thus leads to an increasing trend in the analytical prediction of  $\gamma_{ri}/\gamma_{ri}$ .

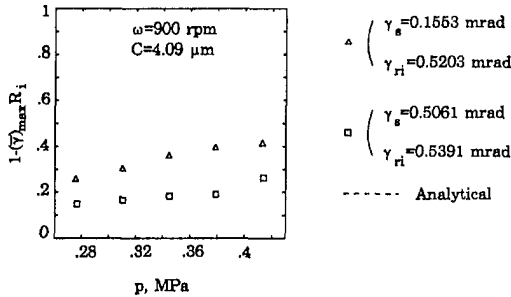
In spite of the poor correlation, however, the absolute values of the experimental and analytical  $\gamma_{ri}/\gamma_{ri}$  agree well ( $e_1 = 13.82$  percent and  $e_2 = 1.04$  percent). As  $\omega$  increases, both the experimental and analytical  $\gamma_{rs}/\gamma_{rs}$  decrease somewhat ( $r_1 = 0.495$  and  $r_2 = 0.534$ ) ( $e_1 = 7.67$  percent and  $e_2 = 8.14$  percent). The operation map shows that the seal operated more safely (away from contact) for the low  $\gamma_s$  than for the high  $\gamma_s$ , and also that generally the seal operated more safely at a higher  $\omega$  because the gyroscopic couple aligns the rotor with respect to the axis of shaft rotation more effectively, and thereby decreases the value of  $(\bar{\gamma}_{max})_{ri}$ .

Results for  $C = 3.88, 4.09, 4.28, 4.47, \text{ and } 4.69 \mu\text{m}$  for the small  $\gamma_s$ , and for  $C = 3.88, 4.09, 4.28, 4.51, \text{ and } 4.66 \mu\text{m}$  for



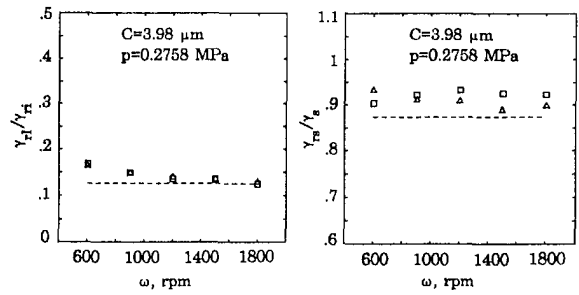
(a)

(b)



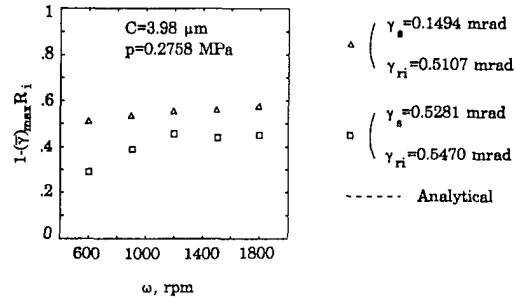
(c)

Fig. 5 (a) Dynamic transmissibility, (b) static transmissibility, and (c) operation map for  $\beta = 11.209$  mrad when  $p$  varies, keeping  $\omega = 900$  rpm and  $C = 4.09$   $\mu\text{m}$  constant



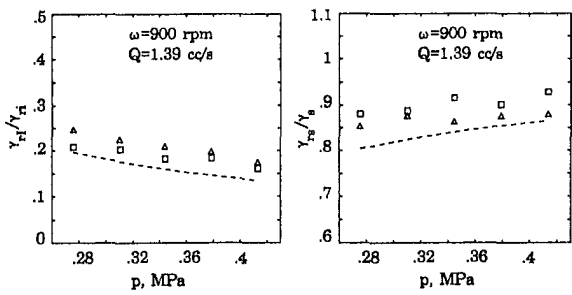
(a)

(b)



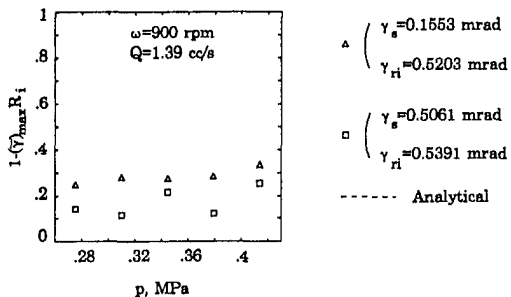
(c)

Fig. 7 (a) Dynamic transmissibility, (b) static transmissibility, and (c) operation map for  $\beta = 4.902$  mrad when  $\omega$  varies, keeping  $C = 3.98$   $\mu\text{m}$  and  $p = 0.2758$  MPa constant



(a)

(b)



(c)

Fig. 6 (a) Dynamic transmissibility, (b) static transmissibility, and (c) operation map for  $\beta = 11.209$  mrad when  $p$  varies, keeping  $\omega = 900$  rpm and  $Q = 1.39$  cc/s constant

the large  $\gamma_s$ , keeping  $\omega = 900$  rpm and  $p = 0.2758$  MPa constant, are shown in Fig. 4. As  $C$  increases, both the experimental and analytical  $\gamma_{ri}/\gamma_{ri}$  increase ( $r_1 = 0.069$  and  $r_2 = 0.880$ ) ( $e_1 = 19.3$  percent  $e_2 = 12.54$  percent), and conversely, both the experimental and analytical  $\gamma_{rs}/\gamma_s$  decrease ( $r_1 = 0.890$  and

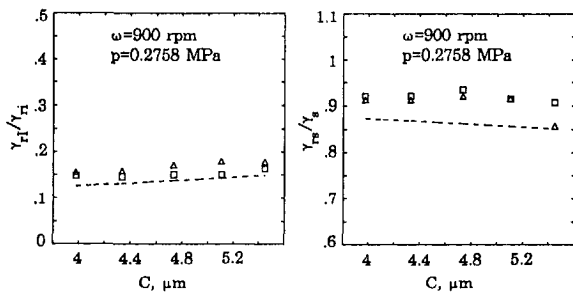
$r_2 = 0.019$ ) ( $e_1 = 5.64$  percent and  $e_2 = 8.16$  percent). This is because at given  $\omega$  and  $p$ , increasing  $C$  has the effect of decreasing the fluid film stiffness [see Eq. (A2)]. The operation map shows that generally, the seal operated more safely as  $C$  increased.

Results for  $p = 0.2758, 0.3103, 0.3447, 0.3792,$  and  $0.4137$  MPa, keeping  $\omega = 900$  rpm and  $C = 4.09$   $\mu\text{m}$  constant, are shown in Fig. 5. As  $p$  increases, both the experimental and analytical  $\gamma_{ri}/\gamma_{ri}$  decrease ( $r_1 = 0.914$  and  $r_2 = 0.766$ ) ( $e_1 = 25.86$  percent and  $e_2 = 16.08$  percent), and conversely, both the experimental and analytical  $\gamma_{rs}/\gamma_s$  increase ( $r_1 = 0.914$  and  $r_2 = 0.766$ ) ( $e_1 = 7.05$  percent and  $e_2 = 6.04$  percent). This is due to an increasing fluid film stiffness where at given  $\omega$  and  $C$ , increasing  $p$  has the effect of increasing the fluid film stiffness [see Eq. (A2)]. The operation map shows that the seal operates more safely as  $p$  increases.

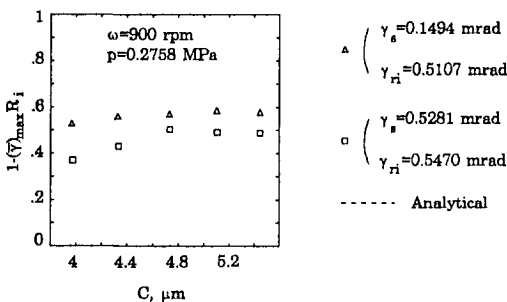
Results for  $p = 0.2758, 0.3103, 0.3447, 0.3792,$  and  $0.4137$  MPa, keeping  $\omega = 900$  rpm and  $Q = 1.39$  cc/s, are shown in Fig. 6. Increasing  $p$ , while keeping the leakage constant, has the effect of decreasing  $C$ . The calculated seal clearances corresponding to the above tested pressures are  $C = 4.09, 3.85, 3.66, 3.49,$  and  $3.34$   $\mu\text{m}$ . As the fluid film stiffness increases due to increasing  $p$  and decreasing  $C$ , both the experimental and analytical  $\gamma_{ri}/\gamma_{ri}$  decrease ( $r_1 = 0.995$  and  $r_2 = 0.929$ ) ( $e_1 = 22.96$  percent and  $e_2 = 13.52$  percent). Conversely, both the experimental and analytical  $\gamma_{rs}/\gamma_s$  increase ( $r_1 = 0.714$  and  $r_2 = 0.861$ ) ( $e_1 = 3.85$  percent and  $e_2 = 7.17$  percent). The operation map shows that generally the seal operated more safely as  $p$  increased and  $C$  decreased because either trend contributes to a higher fluid film stiffness.

**Small Coning.** The coning,  $\beta$ , was  $4.902$  mrad ( $\bar{\beta} = 31.13$  for  $C = 4.0$   $\mu\text{m}$ ). A small value,  $\gamma_s = 0.1494$  mrad, was tested with  $\gamma_{ri} = 0.5107$  mrad, and a large value,  $\gamma_s = 0.5281$  mrad, was tested with  $\gamma_{ri} = 0.5470$  mrad.

Results for  $\omega = 600$  to  $1800$  rpm in increments of  $300$  rpm, keeping  $C = 3.98$   $\mu\text{m}$  and  $p = 0.2758$  MPa constant, are shown in Fig. 7. As  $\omega$  increases, the experimental  $\gamma_{ri}/\gamma_{ri}$  decreases

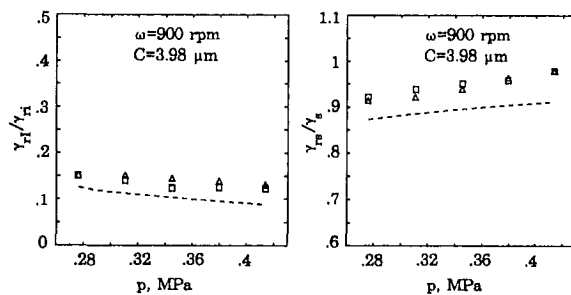


(a) (b)

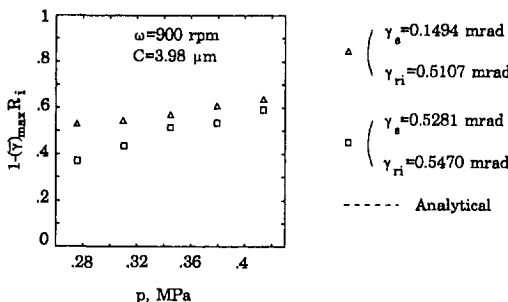


(c)

**Fig. 8 (a) Dynamic transmissibility, (b) static transmissibility, and (c) operation map for  $\beta = 4.902$  mrad when  $C$  varies, keeping  $\omega = 900$  rpm and  $p = 0.2758$  MPa constant**



(a) (b)



(c)

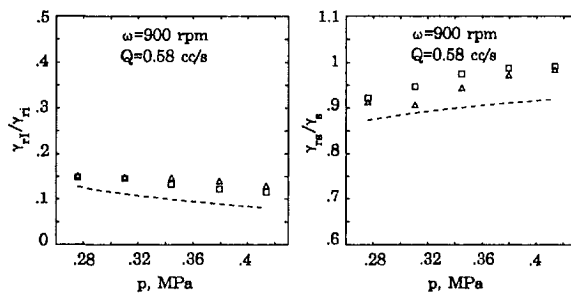
**Fig. 9 (a) Dynamic transmissibility, (b) static transmissibility, and (c) operation map for  $\beta = 4.902$  mrad when  $p$  varies, keeping  $\omega = 900$  rpm and  $C = 3.98$   $\mu\text{m}$  constant**

where the theoretical transmissibility decreases almost unnoticeably ( $r_1 = 0.516$  and  $r_2 = 0.485$ ) ( $e_1 = 14.51$  percent and  $e_2 = 11.44$  percent). As  $\omega$  increases for the low and high  $\gamma_s$ , the experimental  $\gamma_{rs}/\gamma_s$  decreases and somewhat increases, respectively. But the theoretical transmissibility increases slightly ( $r_1 = -0.610$  and  $r_2 = 0.116$ ) ( $e_1 = 3.90$  percent and  $e_2 = 5.16$  percent). Once again the poor correlation may be explained to be the result of uncontrolled temperature effects in calculating the O-rings stiffness. The operation map shows that the seal operates more safely due to the gyroscopic effect as  $\omega$  increases.

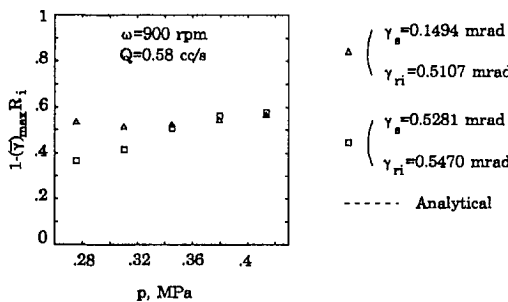
Results for  $C = 3.98, 4.33, 4.74, 5.11,$  and  $5.45$   $\mu\text{m}$ , keeping  $\omega = 900$  rpm and  $p = 0.2758$  MPa constant, are shown in Fig. 8. As  $C$  increases, both the experimental and analytical  $\gamma_{rl}/\gamma_{ri}$  increase ( $r_1 = 0.956$  and  $r_2 = 0.755$ ) ( $e_1 = 17.42$  percent and  $e_2 = 9.08$  percent). As  $C$  increases, the experimental  $\gamma_{rs}/\gamma_s$  decreases slightly but the analytical transmissibility decreases more sharply ( $r_1 = 0.644$  and  $r_2 = 0.489$ ) ( $e_1 = 4.70$  percent and  $e_2 = 6.35$  percent). The operation map shows that the seal operates more safely as  $C$  increases.

Results, for  $p = 0.2758, 0.3103, 0.3447, 0.3792,$  and  $0.4137$  MPa, keeping  $\omega = 900$  rpm and  $C = 3.98$   $\mu\text{m}$  constant, are shown in Fig. 9. As  $p$  increases, both the experimental and analytical  $\gamma_{rl}/\gamma_{ri}$  decrease ( $r_1 = 0.951$  and  $r_2 = 0.929$ ) ( $e_1 = 27.23$  percent and  $e_2 = 21.05$  percent), and conversely, both the experimental and analytical  $\gamma_{rs}/\gamma_s$  increase ( $r_1 = 0.967$  and  $r_2 = 0.985$ ) ( $e_1 = 5.18$  percent and  $e_2 = 5.85$  percent). The operation map shows that the seal operates more safely as  $p$  increases.

Results, for  $p = 0.2758, 0.3103, 0.447, 0.3792,$  and  $0.4137$  MPa, keeping  $\omega = 900$  rpm and  $Q = 0.58$  cc/s, are shown in Fig. 10. The calculated seal clearances corresponding to the above tested pressures are  $C = 3.98, 3.75, 3.56, 3.40,$  and  $3.25$   $\mu\text{m}$ . As  $p$  increases and  $C$  decreases, both the experimental and analytical  $\gamma_{rl}/\gamma_{ri}$  decrease ( $r_1 = 0.905$  and  $r_2 = 0.973$ ) ( $e_1 = 30.28$  percent and  $e_2 = 24.13$  percent), and conversely, the experimental and analytical  $\gamma_{rs}/\gamma_s$  increase ( $r_1 = 0.937$  and  $r_2 = 0.987$ ) ( $e_1 = 4.99$  percent and  $e_2 = 6.87$  percent). The operation map shows that the seal operates more safely as  $p$  increases and  $C$  decreases.



(a) (b)



(c)

**Fig. 10 (a) Dynamic transmissibility, (b) static transmissibility, and (c) operation map for  $\beta = 4.902$  mrad when  $p$  varies, keeping  $\omega = 900$  rpm and  $Q = 0.58$  cc/s constant**

The optimal dimensionless coning angle (Green, 1987), at which the angular fluid film stiffness is maximized, is  $(\beta)_{opt} = 2/[\mathbf{R}_i(1 - \mathbf{R}_i)]$ , and in the present test rig  $(\beta)_{opt} = 12.5$ . Since the low  $\beta$  ( $\beta = 31.13$ ) was closer to the optimal coning angle than the high  $\beta$  ( $\beta = 69.44$ ), the fluid film stiffness at the low  $\beta$  was bigger than that at the high  $\beta$ . Therefore,  $(\gamma)_{\max}$  at the low  $\beta$

was expected to be smaller than that at the high  $\beta$ . For that reason, it was expected that the seal would operate more safely at the low  $\beta$  than at the high  $\beta$ . This can exactly be confirmed by observing the operation maps, where the seal operated more safely at the low  $\beta$  than at the high  $\beta$  for similar operating conditions. The comparison also indicates that generally, the seal operated more safely at the low  $\gamma_s$  than at the high  $\gamma_s$ , as expected.

Moreover, by definition the transmissibilities, Eq. (1), are ratios and are supposed to be independent of the forcing function,  $\gamma_{ri}$ , and  $\gamma_s$ . Indeed, by examining the experimental results in Figs. 3 through 10, it can be seen that differences between the experimental transmissibilities at low and high values of  $\gamma_s$  are minor.

For all test results the differences between the experimental and analytical dynamic transmissibilities are 15.64 percent on average (with a standard deviation of 7.58 percent) for the large coning, and 19.39 percent (with a standard deviation of 7.58 percent) for the small coning. The differences between the experimental and analytical static transmissibilities are 6.72 percent (with a standard deviation of 1.47 percent) for the large coning, and 5.37 percent (with a standard deviation of 0.95 percent) for the small coning. These differences are very reasonable considering the fact that the theoretical transmissibilities were obtained from a linearized analysis. But what is of more significance is that the trends of the experimental and theoretical results are almost always alike. The overall correlation coefficient between the experimental and analytical results is 0.837 (except for the cases of operating conditions where  $\omega$  varied and the other parameters were kept constant). It can be confidently stated that overall there is very good agreement between the analytically predicted transmissibilities and the experimental ones for the operation conditions considered here.

## Conclusions and Recommendations

In this work the steady-state dynamic behavior of the FMR seal was experimentally investigated at various operating conditions, and the results were given in terms of the dynamic and static transmissibilities, and operation maps. The experimental and analytical dynamic and static transmissibilities disagreed somewhat in trends in one set of operating conditions when the shaft speed,  $\omega$ , increased, while keeping the seal clearance and pressure constant. That may be explained by the fact that the support stiffness of the O-rings was predicted to increase as  $\omega$  increases under constant temperature conditions. However, the temperature actually increased with speed because of friction in the other rig parts. Therefore, this model resulted in an overestimation of the actual support stiffness. At the other sets of operating conditions where the support stiffness was kept constant (and where  $\omega$  was kept constant), the experimental and analytical dynamic and static transmissibilities agreed very well. Therefore, it is concluded that the theoretical work by Green (1989, and 1990) predicted well the dynamic behavior of the FMR seal. Comparison of the operation maps suggests that the combination of seal operating parameters that maximize the fluid film stiffness is optimal for a noncontacting seal operation.

The dynamic behavior of the O-rings of the support system is very unpredictable because of the uncontrolled lubrication and temperature conditions. They are the most probable elements that contribute to the differences between the experimental and theoretical results, and the inconsistency of the experimental results from one test to another. Therefore, a support mechanism to replace the O-rings in favor of diaphragms or metal bellows would potentially improve the consistency and repeatability of the results.

In the test rig, most of the heat generation originated at the

contacting seal and the rig became hot in a relatively short time when the shaft speed increased beyond 1800 rpm. For that reason, most of the tests were performed at 900 rpm at which the heat generation was moderate. In addition, the FMR seal was tested at relatively low pressures, which helped to confine the leakage at the sealing dam. However, noncontacting mechanical face seals used in modern high performance turbomachinery operate under higher speeds and higher pressures. Therefore, it is recommended that a future test of the FMR seal be performed at higher speeds and higher pressures. To accomplish this, a redesign of the test rig will be necessary to eliminate the use of the contacting seal and cool the system.

Since there is overall very good agreement between the analytical and experimental results of the dynamic behavior of the FMR seal, it supports the advantages of the FMR seal over the FMS seal as found by Green (1989). Nevertheless, the engineering of FMR seals for high speed applications has to account for the vibration of other seal and system components, such as springs or bellows.

## Acknowledgment

This work was supported in part by the National Science Foundation under grant number MSM-8619190. This support is gratefully acknowledged. The authors would like to thank Mr. Ariel Trau (of the Israel Armament Development Authority) and Dr. Scott Bair (of Georgia Tech) who helped in the design and construction of a prototype test rig.

## References

- Denny, D. F., 1961, "Some Measurement of Fluid Pressures Between Plane Parallel Trust Surfaces with Special Reference to the Behavior of Radial Face Seals," *Wear*, Vol. 4, No. 1, pp. 64-83.
- Etsion, I., 1991, "Mechanical Face Seal Dynamics 1985-1989," *The Shock and Vibration Digest*, Vol. 23, pp. 3-7.
- Green, I., and Etsion, I., 1985, "Stability Threshold and Steady-State Response of Noncontacting Coned-Face Seals," *ASLE Trans.*, Vol. 28, No. 4, pp. 449-460.
- Green, I., 1987, "The Rotor Dynamic Coefficients of Coned-Face Mechanical Seals with Inward or Outward Flow," *ASME JOURNAL OF TRIBOLOGY*, Vol. 109, 1, pp. 129-135.
- Green, I., 1989, "Gyroscopic and Support Effects on the Steady-State Response of a Noncontacting Flexibly Mounted Rotor Mechanical Face Seal," *ASME JOURNAL OF TRIBOLOGY*, Vol. 111, pp. 200-208.
- Green, I., 1990, "Gyroscopic and Damping Effects on the Stability of a Noncontacting Flexibly Mounted Rotor Mechanical Face Seal," *Dynamics of Rotating Machinery*, Hemisphere Publishing Company, pp. 153-173.
- Lee, A. S., 1992, "Experimental Investigation of a Noncontacting Flexibly Mounted Rotor Mechanical Face Seal," Ph.D. Thesis, Georgia Institute of Technology, Atlanta, GA.
- Lee, A. S., and Green, I., 1994a, "Physical Modeling and Data Analysis of the Dynamic Response of a Flexibly Mounted Rotor Mechanical Seal," *ASME JOURNAL OF TRIBOLOGY*, published in this issue, pp. 130-135.
- Lee, A. S., and Green, I., 1994b, "Higher Harmonic Oscillations in a Noncontacting FMR Mechanical Face Seal Test Rig," *ASME Journal of Vibration and Acoustics*, Vol. 116, 2, pp. 161-167.
- Lee, A. S., and Green, I., 1994c, "Rotordynamics of a Mechanical Face Seal Riding on a Flexible Shaft," *ASME JOURNAL OF TRIBOLOGY*, Vol. 116, 2, pp. 345-351.
- Metcalf, R., 1981, "Dynamic Tracking of Angular Misalignment in Liquid-Lubricated End-Face Seals," *ASLE Transactions*, Vol. 24, No. 4, pp. 509-526.
- Salant, R. F., and Blasbalg, D. A., 1991, "Dynamic Behavior of Two-Phase Mechanical Face Seals," *ASLE Tribology Trans.*, Vol. 34, No. 1, pp. 122-130.
- Yasuna, J. A., and Hughes, W. F., 1992, "Squeeze Film Dynamics of Two-Phase Seals," *ASME JOURNAL OF TRIBOLOGY*, Vol. 114, No. 2, pp. 236-246.

## APPENDIX

The geometry of the 0.5198 kg rotor produced a polar moment of inertia,  $I_p = 4.1619 \times 10^{-4} \text{ kg} \cdot \text{m}^2$ , and a transverse moment of inertia,  $I_t = 2.8032 \times 10^{-4} \text{ kg} \cdot \text{m}^2$ . The outer radius was  $r_o = 20.32 \text{ mm}$ , and the radius ratio was  $R_t = 0.8$ . The rotor geometry rendered a balance ratio of 0.5 assuming flat faces

and unpressurized rotor chamber (see Fig. 2). The water viscosity,  $\mu$ , was 0.8935 mPa·s at 25°C.

The transmissibilities of Eq. (1) are in the angular mode. Therefore, only the angular rotordynamic coefficients are needed here. The support stiffness and damping coefficients as derived by Lee and Green (1994a) are

$$K_s = 5.346 + \frac{146.1\omega^2}{36.36 + \omega^2} \text{ [N}\cdot\text{m/rad]}$$

$$D_s = \frac{881.4}{36.36 + \omega^2} \text{ [N}\cdot\text{m}\cdot\text{s/rad]} \quad (\text{A1})$$

giving coefficients  $K_s$  and  $D_s$  as functions of  $\omega$  [rad/s].

The linearized fluid film dynamic coefficients of the FMR seal were derived by Green (1987). Hence,

$$K_f = \pi p \frac{r_o^4}{C} (\bar{\beta} R_i - 1) E_o^2$$

$$D_f = 12\pi\mu \frac{r_o^6}{C^3} (1 - R_i^2) R_m^3 G_o \quad (\text{A2})$$

where  $p$  is the pressure differential across the sealing dam,  $R_m = (1 + R_i)/2$ , is the dimensionless seal mean radius, and

$$E_o = \frac{(1 - R_i) R_m}{2 + \bar{\beta}(1 - R_i)}$$

$$G_o = \frac{\ln[1 + \bar{\beta}(1 - R_i)] - \frac{2\bar{\beta}(1 - R_i)}{2 + \bar{\beta}(1 - R_i)}}{\bar{\beta}^3(1 - R_i)^2}$$